The Egyptian Journal of Hospital Medicine (April 2023) Vol. 91, Page 3885-3895

Gold Nanoparticle Biosynthesis-Mediated *Acinetobacter ƀaumannii* as a Cytotoxic and Apoptosis Inducer in Prostate Cancer Cell Lines

Intesar H. Al-Abdeli*, Esam J. Al-kalifawi
Department of Biology, College of Education for Pure Science,
Ibn-Al-Haitham University of Baghdad, Baghdad, Iraq
***Corresponding author: Intesar H. Al-Abdeli, Mobile:** (+20) 01140292959,
Email: Intessar.Hameed1102a@ihcoedu.uobaghdad.edu.iq

ABSTRACT

Background: Gold nanoparticles (AuNPs), unlike chemotherapy, may destroy cancer cells without harming normal cells.

Objective: For the first time, *Acinetobacter* (*A.*) *baumannii*-biosynthesized AuNPs (Ab-AuNPs) were evaluated for anticancer properties.

Materials and methods: The Ab-AuNPs were characterized by UV-visible spectroscopy, TEM, FE-SEM, AFM, XRD analysis, and FTIR. The MTT assay was used to determine the antiproliferative efficacy of the Ab-AuNPs at different concentrations against prostate cancer (PC3) and human breast normal cell line (MCF-10). Potential apoptotic-mediated cell death was investigated using acridine orange and propidium iodide staining and mitochondrial membrane potential (MMP).

Results: Biosynthesized Ab-AuNP had a zeta potential below 30 mV at -22 mV, suggesting particles stability with no aggregation. The average size was estimated at 66 nm (range 20-90 nm). Ab-AuNPs inhibited PC3 cell proliferation dose-dependently, with no adverse effect on MCF-10 cells. The mean lethal dose (IC_{50}) was 13.72 µg/mL, and the maximal inhibitory concentration was 25.50 mg/mL (57.33% and 80.67%, respectively). Examining PC3 cancer cells treated with Ab-AuNPs at IC_{50} for 24 hours by flow cytometry revealed an increase in apoptosis that resulted in the disruption of the membrane and vacuoles of the lysosomes, which corresponded with the depletion of MMP. This was in contrast to MCF-10 AuNPs-treated cells, which showed no adverse effects.

Conclusions: Producing gold nanoparticles in an *A. baumannii* broth culture is simple, inexpensive, and non-toxic to healthy cells. They showed anticancer effects by inducing apoptosis, making them a potential effective anticancer agent.

Keywords: Gold nanoparticles, *Acinetobacter baumannii*, Anti-cancer activity, Apoptosis activity.

INTRODUCTION

The use of biological systems in nanoscience has given birth to the name nanobiotechnology, which modulates entities in the 1–100 nm range using biological systems or for the benefit of natural systems [(1)]. It is a field Bio sourced synthesis of nanomaterials mediated by microorganisms and plants. Bio-sourced synthesis of nanomaterials through microorganisms and plant-based mediators is a growing field [(2)]. Many bacteria, the most prevalent species in the biosphere, have been shown to create extracellular and intracellular metallic nanoparticles [(3)]. *Acinetobacter* (*A. ƀaumannii*) has been suggested because it is widespread in the surrounding environment. Acinetobacter is a diverse group of organisms ubiquitous in nature [(4)]. Its high forming capacity allows it to form biofilms and withstand extreme conditions [(5)]. This group is known to resist various metal ions and antibiotics [(6)].

The biosynthesis of gold nanoparticles (AuNPs) would benefit from developing clean, non-toxic, and environmentally friendly procedures for microorganisms from bacteria to fungi [(7)].

The simplest way to produce nanoparticles is to reduce the respective salts [(8)]. Bacteria have always been organisms of choice due to their unique property of creating various enzymes for chemical detoxification and energy-dependent ion efflux, involved in the decrease and stability of metallic nanoparticles [(9)].

There are several uses for AuNPs in cancer diagnostics and therapy, drug delivery, and gene therapy [(10)]. AuNPs are the most commonly used metal nanoparticles due to their morphology, dimensions, excellent optical and electronic properties, high biocompatibility, and stability [(11)]. Cancer is one of the leading causes of death worldwide, affecting over 11 million people annually [(12)].

Including prostate cancer is a tumor that forms in the male prostate (a little gland with a walnut-like form) that produces semen, which supplies nutrients and transports sperm, and the most common cancer in men is prostate cancer [(13)]. After AuNPs enter most cancer cells, a series of processes evolve from the loss of migration stability, the onset of unstable oxidation states, and waves of free radicals that disrupt and expand the nuclear membrane of the nucleus. Initially, mitochondria unfold to increase oxidative stress within the cell [(14)].

The aim of current study was to demonstrate the biosynthesis of AuNPs using *A. ƀaumannii* broth cultures and measuring its *in vitro* cytotoxic effects on tumor cell lines prostate cancer (PC3) and comparing them with the normal human cell line MCF-10, to evaluate its potential therapeutic anticancer activity and its apoptosis induction in prostate cancer cell lines.

Received: 04/08/2022
Accepted: 05/10/2022

MATERIALS AND METHODS

Detection of *A. baumannii*

In this study, AuNPs were synthesized by growing *A. baumannii* in a broth culture functioned as both a stabilizer and a reducing agent. Isolates of *A. baumannii* were collected in the microbiology laboratories at the Yarmouk Teaching Hospital, Baghdad, Iraq. Gram staining, colony characterization, dye production, blood hemolysis, culturing, such as the growth on nutrient broth and MacConkey agar (Oxoid Ltd., England), and biochemical tests, such as catalase, coagulase, urease, and oxidase, and lastly the VITEC® 2 Compact system (bioMérieux, France) were used to confirm the isolation [15].

Biosynthesis of AuNPs using *A. baumannii*:

AuNPs were produced using the modified method described in **Sabir *et al.*** [16]. Ten milliliters of stock solution of gold chloride ($HAuCl_{l4}.4H_2O$, Merk, Germany) were combined with two milliliters, four milliliters, six milliliters, eight milliliters, and ten milliliters of *A. baumannii* broth culture and heated at 50 °C for 30 minutes on a magnetic hotplate stirrer. Deionized water was then added to bring the total volume to 15 mL.

The resulting mixture was placed in a tube and a 30-minute ultrasonic bath.

Following the development of red dots on the sides of the transparent line inside the Ultrasonic Bath device, the solution's color changed from bright yellow to yellowish-orange. Each time the procedure is carried out, two mL of the bacterial broth culture was added to the gold salt solution, while the other parameters, including the gold salt solution concentration, temperature, time, and pH value, were held constant to produce an orange-colored solution. Changing in the color from light purple to a darker purple indicated the creation of AuNPs (Figure 1).

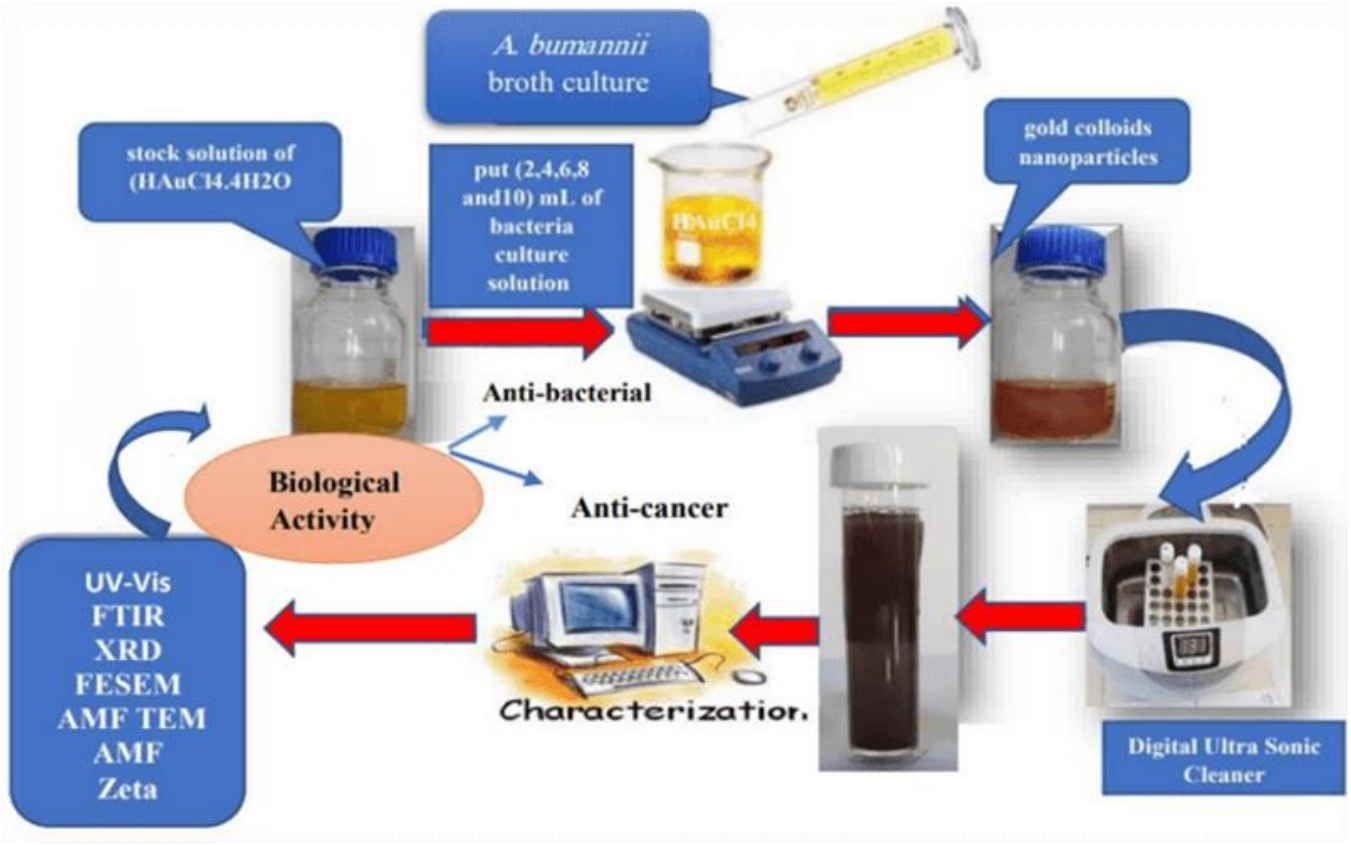

Figure (1): Graphical representation of the steps followed for Acinetobacter baumannii-biosynthesized gold nanoparticles (Ab-NPs)

Characterization of Ab-AuNPs

Ab-AuNPs were characterized using many techniques, UV-Vis spectroscopy (Shimadzu UV-160A , Fourier transform infrared (FTIR) (IRAffinity1Shmadzo), field emission scanning electron microscope (FE-SEM), transmission electron microscope (TEM) (Carl Zeiss, Germany), atomic force microscopy (AFM) (ZEISS Integrated), X-Ray diffraction (XRD) ((Philips PW1730), and Zeta potential measurement.

Identification of the cytotoxic effects of AuNPs

Cancer cell lines

The PC3 prostate cancer line and the MCF-10 normal cell line were kindly provided by the Cell Bank of the Iraqi Center for Cancer and Medical Genetic Research, Baghdad, Iraq. The RPMI-1640 medium (USbiological), was used to cultivate the cell lines. A 10% fetal bovine serum (FBS), 100 mg/mL streptomycin, and 100 units/mL penicillin (Capric Scientific, Germany) were added as supplementations to the medium. At 80% confluence, cells were trypsinized and subcultured twice weekly before being incubated at 73 °C in a humidified environment containing 5% CO_2 [17,18].

Determination of cytotoxicity of Ab-AuNPs using MTT assay

The cytotoxicity test was done based on **Al-Salman *et al.*** [19]. The MTT assay was performed by seeding a 96-well plate with 1×10^5 of PC3 and MCF-10 cells/well grown in RPMI-1640 medium. After 24 hours or when formation a confluent monolayer, cells were treated with 3.1, 6.25, 12.5, 25, and 50 µg/mL Ab-AuNP. After 72 hours, the cells' viability was assessed by removing the medium, adding 2 µg/L MTT, and incubating them for 2.5 hours at 37 °C. After removing the MTT solution, the wells were shaken for 15 minutes at 37 °C with 130 µL of DMSO to break up the crystals. A microplate reader was used to determine the absorbency at 492 nm. The concentration that inhibited growth of 50% of cells (IC_{50}) was determined using the regression analysis.

Acridine orange (AO)–propidium iodide (PI (staining

The ability of Ab-AuNP nanoparticles to induce apoptosis was evaluated using AO/PI double staining as previously described [19]. PC3 and MCF-10 cells seeded 24 hours in 12-well glass slides were exposed to Ab-AuNP at IC_{50} concentration for 24, 48, and 72 hours. Following two PBS washes, dual fluorescent dyes were added to each well and examined using a fluorescence microscope.

Mitochondrial membrane analysis

Rh123, a noncytotoxic fluorescent dye isolated from mitochondria, is used to identify key apoptotic events in cells treated with Ab-AuNPs. This dye was used before and after Ab-AuNP treatment to investigate mitochondrial cell membrane potential. After 24 hours seeding of the PC3 and MCF-10 cells in 96-well plates, the cells were treated with Ab-AuNPs at the IC_{50} concentration and labeled with 2.5 M Rh123 dye for 1 hour at 37 °C. Trypsin-EDTA at 0.5% was applied to separate the cells, which were centrifuged for 5 minutes at 3000 rpm. Following suspension of cells in FACS buffer and flow cytometric analysis, histograms were generated. Flow cytometric histograms were created following suspension of cells in FACS buffer and counts were made [20].

Ethics approval: Center for Cancer and Medical Genetic Research at Mustansiriyah University in Baghdad, Iraq with the Scientific Committee of the Department of Biology in the College of Education for Pure Science at Ibn-Al-Haitham University in Baghdad, Iraq approved the conduction of this study.

Statistical analysis

The results were statistically analyzed using GraphPad Prism 6 and are shown as the mean ± SD of three replicates for each experiment [21]. The data were analyzed statistically using GraphPad Prism 6, and the results were presented as the mean ± SD of the three independent experiments.

RESULTS

Figure (2) showed how the color changes from yellow to dark violet, evidence of the biosynthesis of Ab-AuNPs using *A. baumannii* broth culture.

Figure (2): Exhibit gold nanodots in suspension. Particle sizes and shapes cause color differences

UV-Visible analysis

The UV-Visible spectrum of Ab-AuNPs biosynthesized using *A. baumannii* broth culture, as seen in figure (3). Ab-AuNPs demonstrated surface plasmon resonance (SPR) bands about 574 nm in UV-Visible spectra.

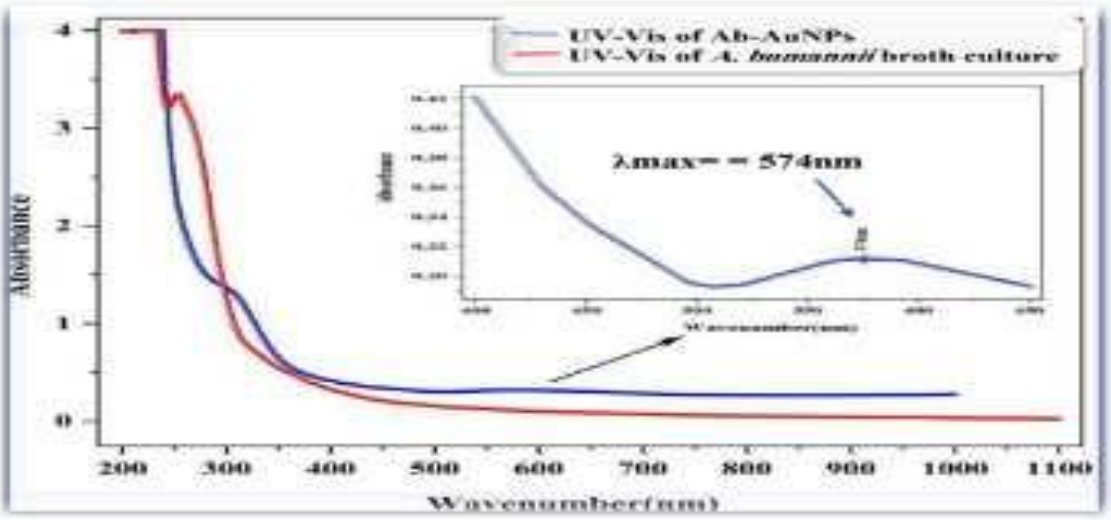

Figure (3): UV-Vis spectrum of Ab-AuNPs colloidal and *A. baumannii* broth culture.

FTIR:

The FT-IR spectra of Ab-AuNPs in figure (4) showed that the main peaks were at 3321.42, 2823.79, 2144.84, and1631.78 cm^{-1}. The large height at 3321.42 cm^{-1} is the relativity O-H stretch of hydrogen-bonded alcohols, phenol, and the N-H stretch of amines or amides. Alkanes, aldehydes, and corrosive carboxylic compounds independently exhibit C=H stretches at 2823.79 cm^{-1}, with C=O stretch at 1631.78 cm^{-1}. The vibration of Ab-AuNP is shown by strong peaks in the region of 578.64-748.38 cm^{1}. This result indicates that Ab-AuNPs were successfully produced [(22)].

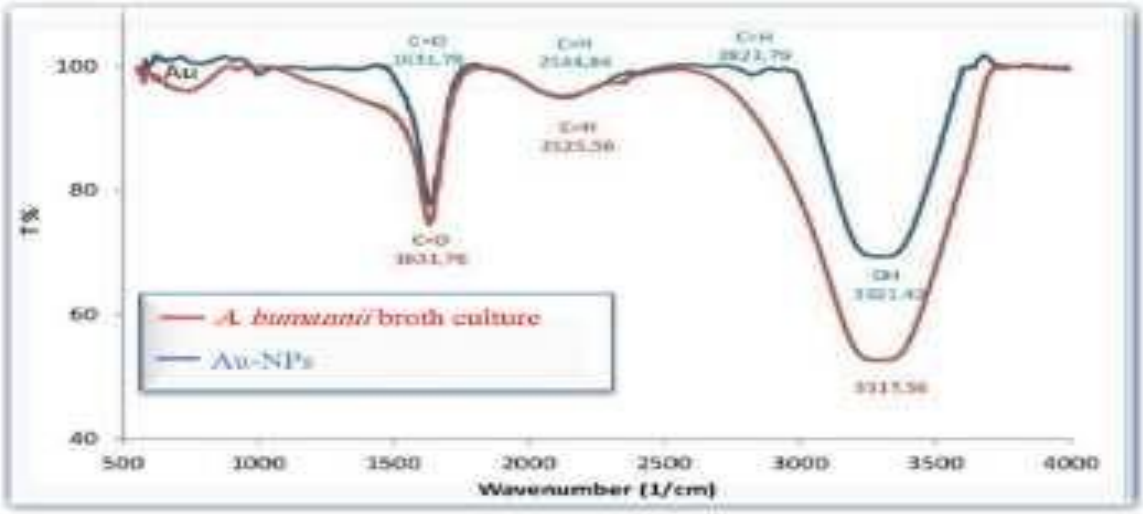

Fig. (4): FTIR spectrum of *A. baumannii* broth culture and (blue) the Ab-AuNPs colloidal.

XRD analysis:

Main peaks are shown in figure (5) at 111, 200, 220, and 311. These correspond to reflections with Bragg angles of 38.18°, 44, 51°, 64.80°, and 77.72° respectively. These findings confirm that the substance under study is, in fact, highly pure AuNPs. In order to calculate the average crystallite size of the Ab-AuNPs arrays, the Debye-Scherrer equation was used.

Figure (5) demonstrated the main peaks at 111, 200, 220, and 311, which are respectively reflections with 2 values of Bragg angles 38.18°, 44, 51°, 64.80°, and 77.72°. These results showed that the analyzed substance is highly pure AuNPs. These findings demonstrated that the substance under study is in fact, highly pure AuNPs. The average crystallite size of the Ab-AuNPs arrays was calculated to be 26.82 nm using the Debye-Scherrer equation [(23)].

D = $K\lambda\beta COS\theta$ [Debye-Scherrer equation]

It elaborates on the connection between XRD peak broadening and crystallite size. Where D is the average size of nanoparticles, K is the Scherrer constant, which has a value of 0.9, Bragg's angle, and the wavelength of the X-ray radiation source, 0.15406 nm.

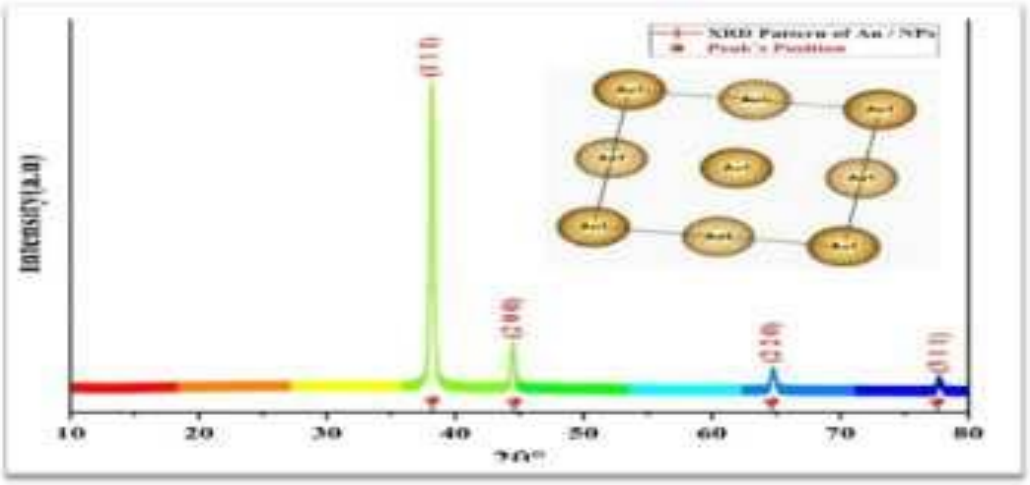

Figure (5): XRD of Ab-AuNPs biosynthesized using *A. baumannii* broth culture.

TEM examination:

Ab-AuNPs ranged in size from 20 to 90 nm, averaging 66 nm (Figures 6 and 7). The reaction starts with the generation of hemispherical Ab-AuNPs. Besides rectangular, triangular, pentagonal, cylindrical, irregular, and polymorphic shapes. Due to the high concentration of reducing factor in the culture broth of *A. baumannii*.

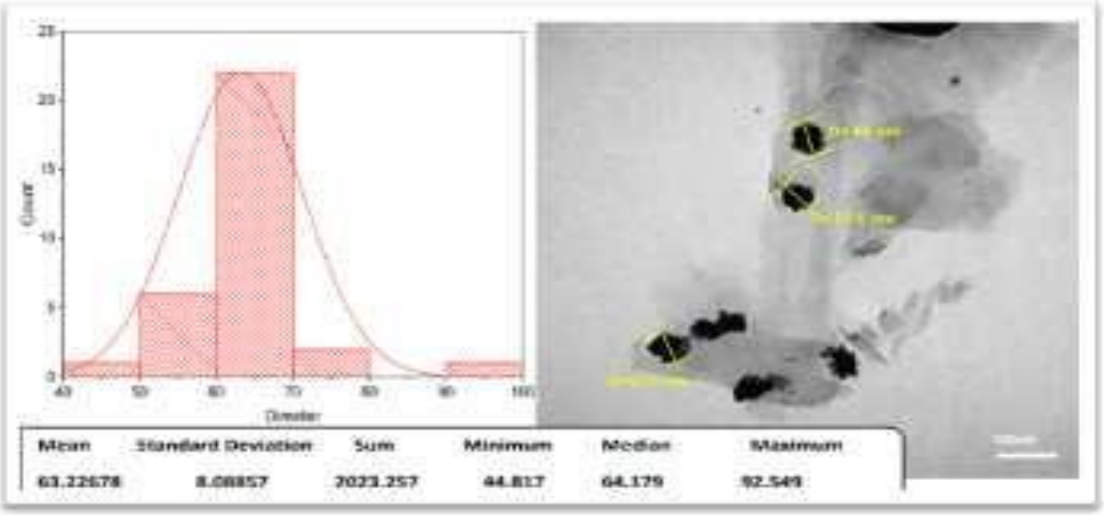

Figure (6): TEM image of biosynthesized AuNPs using *A. baumannii* broth culture, (a) Average diameters of gold nanoparticles, (b) diverse shapes.

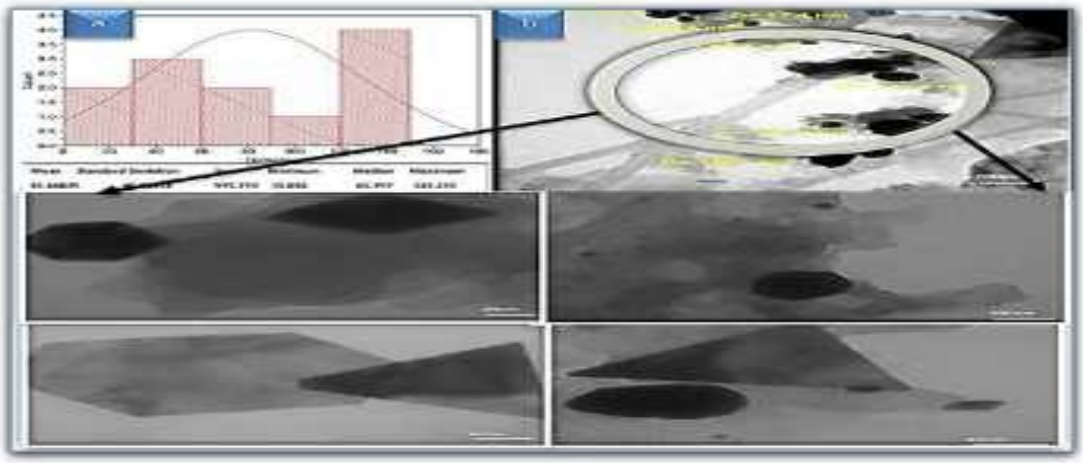

Figure (7): TEM image of biosynthesized Ab-AuNPs using *A. baumannii* broth culture, (a) Average diameters of gold nanoparticles, (b) diverse shapes

FE-SEM:

The FE-SEM results showed that Ab-AuNPs have a spherical form, a high degree of aggregation, and a size that ranges from 66.nm to 363 nm (Figure 8)

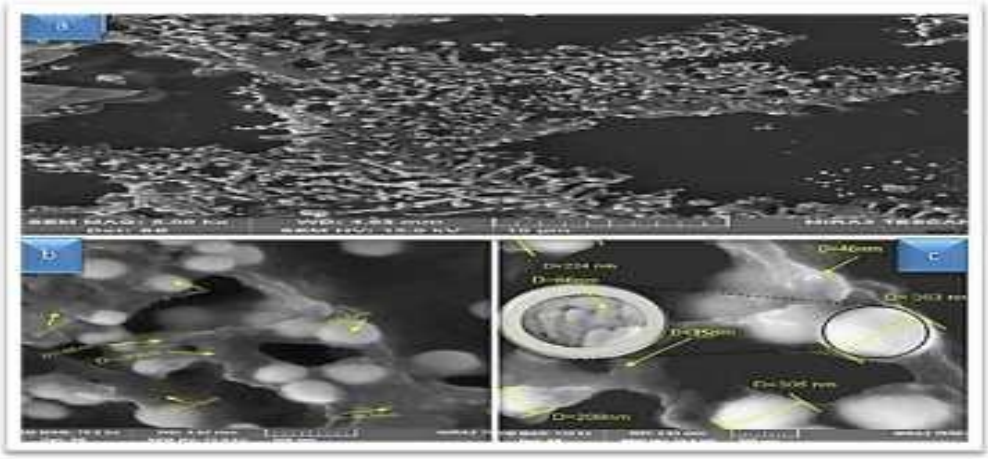

Figure (8): FE-SEM images of biosynthesized Ab-AuNPs using *A. baumannii* broth culture, a, b, c shows shapes of Ab-AuNPs.

AFM analysis:

The size distribution of Ab-AuNP can be seen on the 2D and 3D AFM images. No aggregation or agglomeration was observed in the AFM sample slide sample, showing the high stability of the Ab-AuNPs produced after two months of AuNP synthesis. Ab-AuNPs ranged in size from 15 to 125 nm, with a mean length of 63.82 nm. (Figure 9).

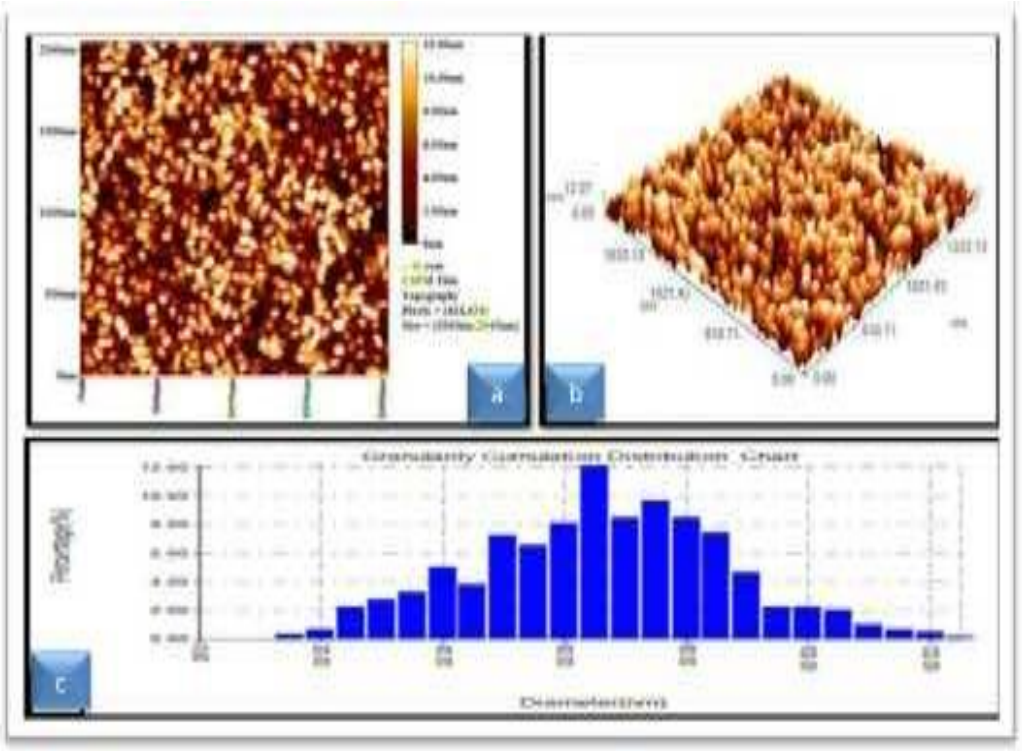

Figure (9): AFM images of biosynthesized Ab-AuNPs using *A. baumannii* broth culture, (a) Two-Dimensional, (b) Three-Dimensional, and (c) Average particle size.

Zeta potential measurements:

Figure (10) showed that the biosynthesized Ab-AuNPs produced by *A. baumannii* broth culture had a zeta potential of -22 mV and less than 30 mV, indicating that the particles are stable and do not aggregate.

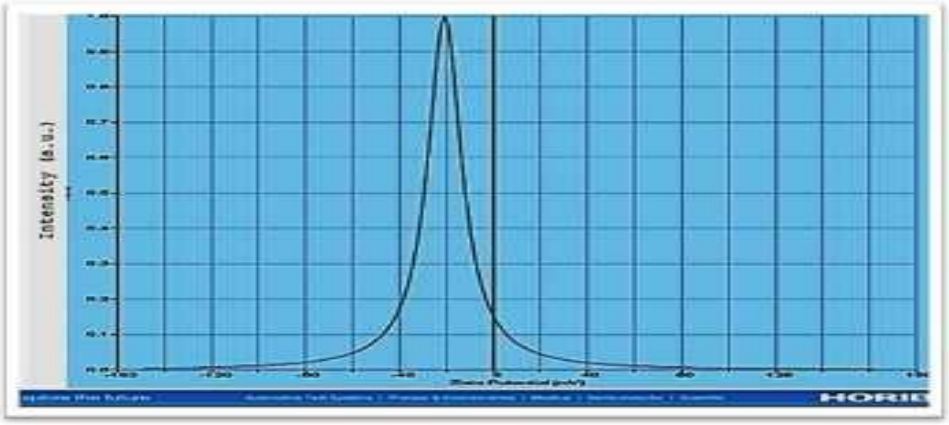

Figure (10): Zeta potential analysis of biosynthesized Ab-AuNPs using *A. baumannii* broth culture.

Evaluation of cytotoxic activity of synthetic Ab-AuNPs

The cytotoxicity of Ab-AuNP on cells under *in vitro* conditions was assessed by the MTT technique in terms of the effect of nanoparticles on cell proliferation. In the current study, results of cytotoxicity of Ab-AuNP against the PC3 cell line showed that the cytotoxicity of Ab-AuNPs increases as the concentration increases (Figure 11).

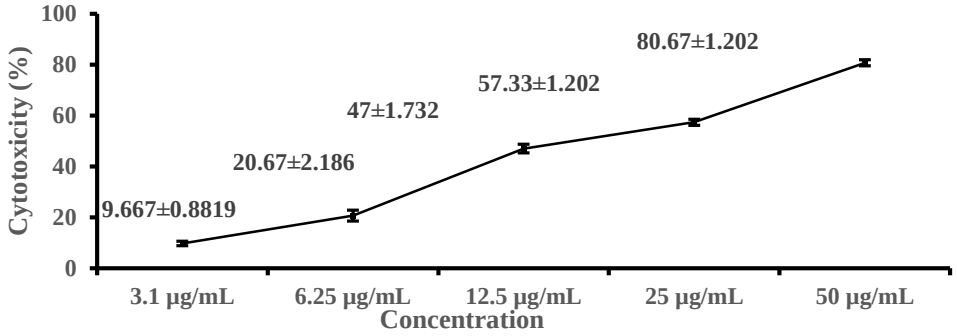

Figure (11): Cytotoxicity effect of biosynthesized Ab-AuNPs using *A. baumannii* broth culture on PC3 cells. IC_{50}= 13.72 µg/mL.

The minimal inhibitory concentration of PC3 cells per reaction with Ab-AuNPs was received at 6.25 µg/mL and 12.5 µg/mL (20.67% and 47.00%, respectively). The calculation of cytotoxicity was as follows:

Inhibition rate (%) = (A- B/A) ×100

Where A is the optical density of the control, and B is the optical density of the samples [(18)].

However, the maximum inhibitory concentration was 25, 50 mg/mL (57.33% and 80.67%); AuNP against the PC3 cancer cell line but not against the normal MCF-10 cell line (Figures 12 & 13).

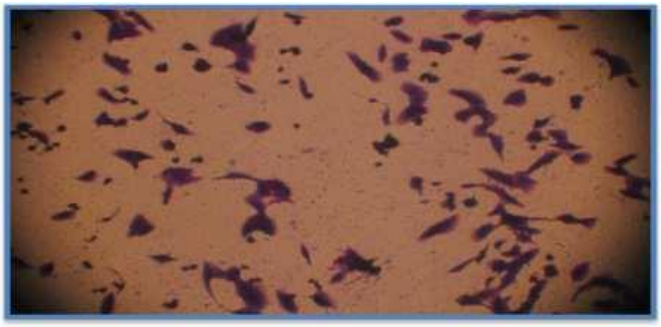

Figure (12): Morphological alterations in PC3 cells after Ab-AuNP treatment

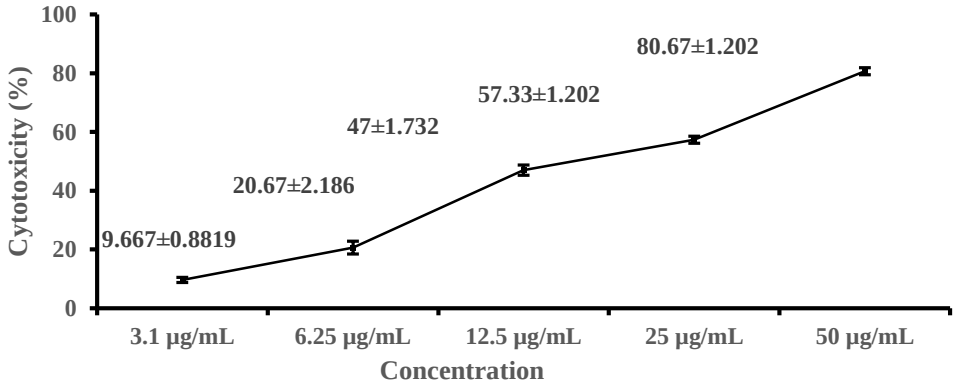

Figure (13): Cytotoxic effect of biosynthesized Ab-AuNPs using *A. baumannii* broth culture on MCF-10 cells. IC_{50}= 13.72 µg/mL.

Cytotoxic effect of synthetic Ab-AuNPs on MCF-10 normal cell lines:

The proliferation of lineage PC3 versus MCF-10 cells was significantly inhibited, as were PC3 line and MCF-10 cells treated with Ab-AuNP simultaneously and under identical conditions, as shown in figure (14).

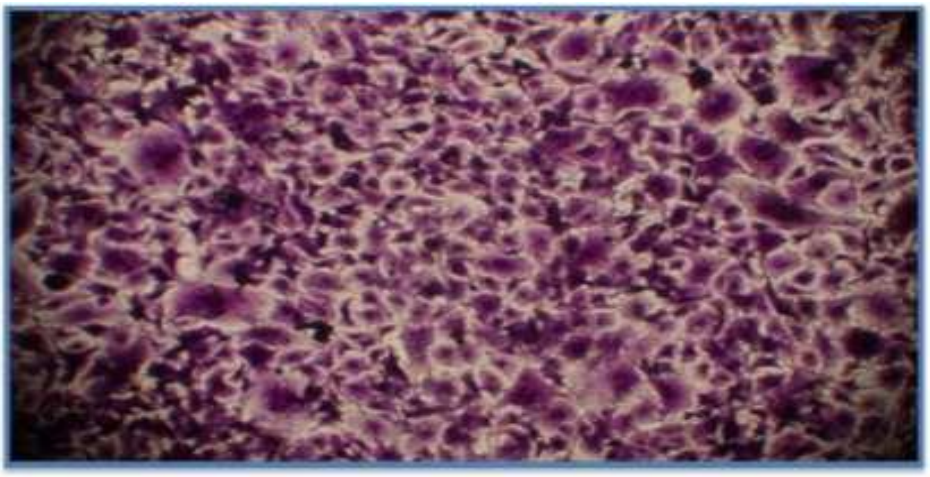

Figure (14): Morphological alterations in MCF-10 cells after Ab-AuNP treatment

AO and PI staining assay:

Dual staining (AO/PI) is a fluorescent combination stain that detects morphological modification in the nucleus by producing distinctive fluorescent colors. Fluorescence dye permeability to the plasma membrane is enhanced in apoptotic cells. Dual cell staining and fluorescence microscopy were used to identify nucleus morphological changes after treating cell lines with the IC50 concentrations of Ab-AuNPs. IC_{50} doses of Ab-AuNPs disrupted lysosome membranes and vacuoles, whereas untreated cells labeled green with AO-PI demonstrated viability (Figure 15).

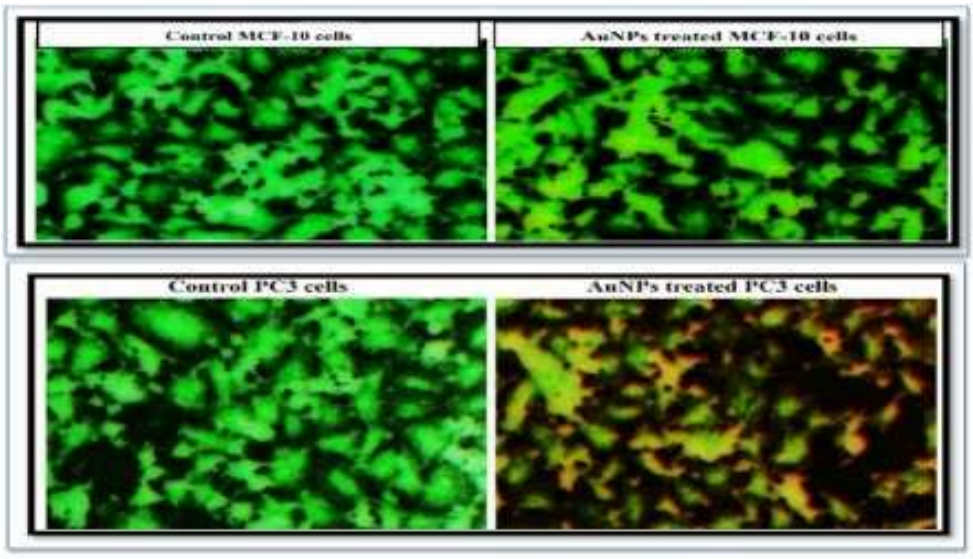

Figure (15): Apoptosis marker in cancer cells, Fluorescence microscopy images of cell lines stained with acridine orange (AO) and propidium iodide (PI). Cells were treated with IC50 concentrations of Ab-AuNPs. Scale bare 30 µm.

Effect of AuNPs on mitochondrial membrane potential of cancer cells

Through cell death stimulation, apoptosis is caused by the mitochondria, which play a significant and crucial part. This organ's changes are marked by the decrease in its membrane potential (Figure 16), releasing cytochrome c protein into the cytoplasm. This study used a flow cytometry assay and followed the manufacturer's instructions to find apoptosis. The decrease in mitochondrial membrane potential in PC3 cells is an important and useful sign of apoptotic cell death [(24)].

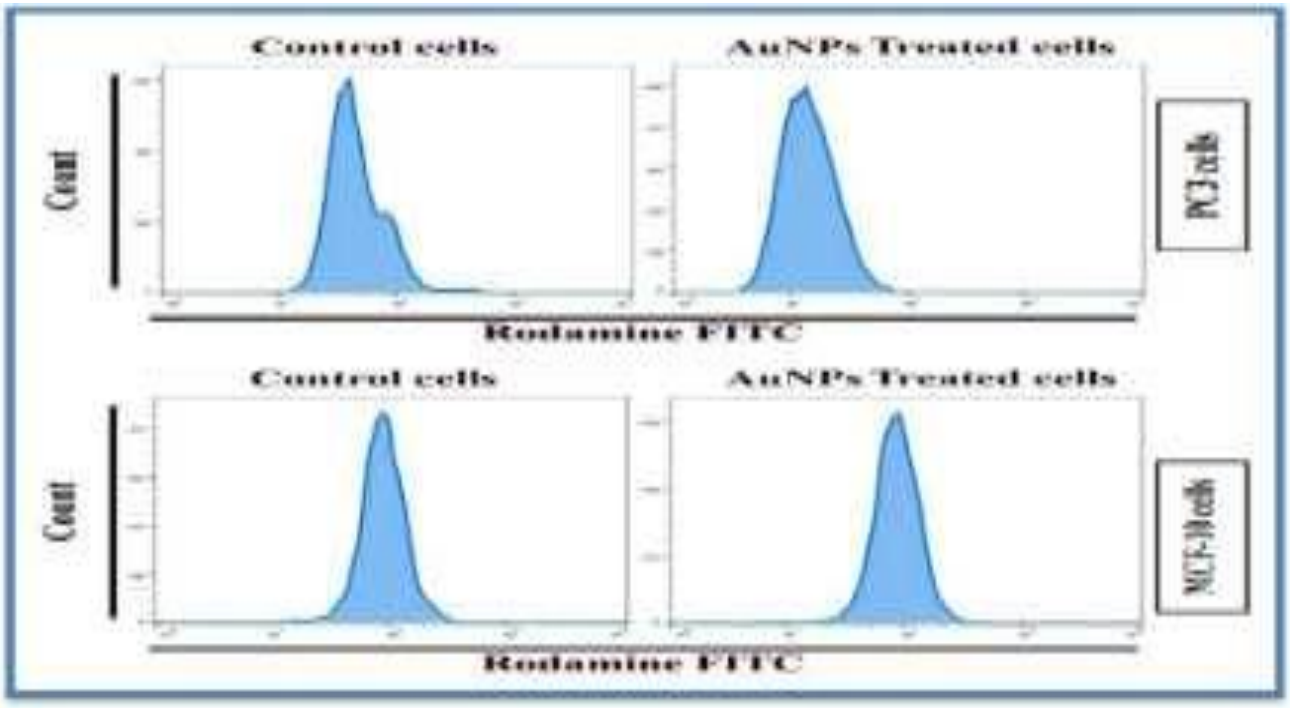

Figure (16): Effect of AuNPs on potential mitochondrial activity.

DISCUSSION

Ab-AuNPs were biosynthesized using the gold solution and *A. baumannii* broth cultures for the first time. Bacterial broth cultures contain polysaccharides, amino acids, peptides, proteins, and enzymes. The color changed from dazzling yellow to dark purple in broth culture, indicating Ab-AuNP synthesis. These chemicals capped and decreased Ab-AuNPs synthesis. These data reveal that metal biotransformation incorporates metals and metal oxides that diminish capping proteins/peptides, reductases, kinins, cytochromes, photokeratitis, or electron shuttles. It supports enzyme-related studies [(25)]. This study gave many broth cultures a constant amount of gold solution. Broth culture increased the color shift, indicating that AuNPs have more reducing and capping agents .This investigation promoted the reaction with a lot of broth medium Similar to **Al-Kalifawi** [(26)].

UV-Visible analysis: Surface plasmon resonance (SPR) bands were seen around 574 nm in the UV-Visible spectra of Au-NPs. The results of this study agree with what reported about how bacteria *Klebsiella pneumonia* were used to make AuNPs with surface plasmon resonance values between 400 and 700 nm. The color change of the solutions from yellow to purple could be used to track the production of gold nanoparticles. This showed that turning Au^{3+} into Au^{0} nanoparticles led to the formation of AuNPs [(27)].

Fourier transforms infrared spectroscopy analysis: Ab-AuNPs were made, and their FTIR spectra showed no functional groups from the *A. baumannii* broth culture in the synthesized Ab-AuNPs showed that during the formation of Ab-AuNPs, some bonds can form, some can break, and some absorbances have decreased because it was used as a capping agent. When AuNPs move, they make sharp peaks between 578.64 and 748.38 cm^{1}. This means that Au-NPs were made correctly [(28)].

X-Ray diffraction analysis: X-Bragg's examination of Ab-AuNPs, similar to a previous study using bacterial and yeast external and intracellular culture supernatants showed four prominent peaks in the XRD spectra [(29)]. The reflection with two Bragg angles, 38.18°, 44.51°, 64.80°, and 77.72° matches the greatest peaks at 111, 200, 220, and 311. These findings indicate extraordinarily pure Ab-AuNPs. The Debye-Scherrer equation calculates the array's Ab-AuNPs' average crystallite size as 26.82 nm. Our results are similar to yeast, bacteria, and plant extract AuNP studies [(30)].

Transmission Electron Microscope analysis (TEM): The wide range of Ab-AuNPs in the solution showed that the Ab-AuNPs made under those conditions were polydispersed. This result is in line with the sample's UV-Vis analysis, in which broad spectrums were formed. Ab-AuNPs were found to have a diameter of between 20 and 90 nm, with an average of 60 nm. During the synthesis process, the magnetic stirrer might have moved in a way that made AuNPs different shapes.

These findings match prior research [31].

Field Emission Scanning Electron Microscope analysis: The results of the FESEM of the biosynthesized gold showed much aggregation in the images. This is because of the heat that was created during the deposition process. It has demonstrated that the Ab-AuNPs, which were about 66 nm to 363 nm in size, were made up of leftover bacteria or proteins with gold nanoparticles, with a cluster that looks like castor plant leaves (Figure 8).

AFM Analysis: Atomic force microscopy measured the size and form of *A. baumannii* broth-biosynthesized Ab-AuNPs (AFM). 2D and 3D AFM images and AuNP size distribution are shown. Ab-AuNPs were 15-128 nm, with an average size of 63.8 nm.

Zeta Potential: Based on the results of the samples, the Zeta Potentials of the synthesized Ab-AuNps were between -22 mV and 30 mV. This could be because the bacteria solution was used as a stabilizer. Bacteria solution comprises magnesium, chloride, potassium, sodium salts of dead bacterial cells, and nutrient broth. The salts break apart when bacteria are analyzed in water, revealing the negative charge. This allows the negative charge of the bacteria to interact with the positive charge of the gold nanoparticles, causing them to stick together.

MTT assay: Synthesized Ab-AuNPs were used to test their cytotoxicity. Ab-AuNPs were tested for anticancer effects by inhibiting malignant cell proliferation. Synthesized Ab-AuNPs were harmful to PC3. While the results did not reveal that Ab-AuNPs generated cytotoxicity in healthy cells (MCF-10). Anticancer phenomena were found by analyzing the nanoparticles' capacity to diminish or block cancer cells, as shown in figure (12). Ab-AuNPs treatment of cancer cell lines (PC3) for 72 hours greatly reduced their proliferative capacity, which is consistent with the findings of studies [32]. According to a survey by **Abdullah and Mohammed** [33], AuNPs significantly impact cancer cells compared to healthy cells. In contrast, the morphology of PC3 cells lines treated with Ab-AuNPs was altered.

Effect of AuNPs on Apoptotic cells: Dual (Ao/Pi) staining is a fluorescent combination stain that detects morphological changes in the nucleus by generating a distinctive luminous color. Apoptotic cells of AO-Pi-PC-3-treated cells increased the plasma membrane's permeability to the fluorescent dye. Ab-AuNPs at IC50 concentrations ruptured lysosomal membranes and vacuoles compared to MCF-10, which exhibited a green stain and indicated survivability.

Effect of AuNPs on potential mitochondrial activity: The manufacturer's instructions identified apoptosis in this work using a flow cytometry technique. The decrease in mitochondrial membrane potential is an essential and crucial signal of apoptotic cell death. Compared to control cells, this is linked to the depletion of mitochondrial membrane potential. Ab-AuNPs were discovered to have strong lethal effects on aberrant cells in local investigations [34]. These results are consistent with these findings. As a result, these nanoparticles may be utilized in researching and developing efficient anticancer drugs.

CONCLUSION

We found that using *A. baumannii* broth culture to make Ab-AuNPs is a relatively safe way to do it because no outside chemicals are used. The process is easy to scale up, and the cost is stable. The anticancer effects of gold nanoparticles showed that they might have the potential to be utilized as a different anticancer treatment agent, pending assuredly more evaluation.

Acknowledgments: The Iraqi Center for Cancer and Medical Genetic Research Cell Bank Director is thankful for supplying us with malignant and normal cell lines, aid, and direction during the research completion period. We thank the Director of Yarmouk Teaching Hospital for offering us *A. baumannii* isolates. We also appreciate the support of the Department of Biology, College of Education for Pure Sciences Ibn Al-Haytham team.

Conflict of interest: The authors declared no conflict of interest.

Sources of funding: This research did not receive any specific grant from funding agencies in the public, commercial, or not-for-profit sectors.

REFERENCES

1. **Sivakami A, Sarankumar R, Vinodha S (2021):** Introduction to Nanobiotechnology: Novel and Smart Applications. In: Pal K. (eds) Bio-manufactured Nanomaterials. Springer, Cham., Switzerland.
2. **Bayda S, Adeel M, Tuccinardi T *et al.* (2019):** The history of nanoscience and nanotechnology: from chemical-physical applications to nanomedicine. Molecules, 25 (1): 112-121.
3. **Qin W, Wang C, Ma Y *et al.* (2020):** Microbe-mediated extracellular and intracellular mineralization: environmental, industrial, and biotechnological applications. https://onlinelibrary.wiley.com/doi/full/ 10.1002/ adma. 201907833
4. **Al-Shaabani M, Al-Ethawi A, Al-Mathkhury H (2020):** Eco-friendly synthesis of gold nanoparticles and study their effect with antibiotics against *Acinetobacter*. The Iraqi Journal of Agricultural Science, 51 (4): 1204-1211.
5. **Al-Shaabani M, Turki A, Al-Mathkhury H (2020):** The antibiofilm efficacy of gold nanoparticles against *Acinetobacter baumannii*: Iraqi Journal of Science, 61 (4): 749-753.
6. **McNeilly O, Mann R, Hamidian M *et al.* (2021):** An emerging concern for silver nanoparticle resistance in *Acinetobacter baumannii* and other bacteria. https://www.frontiersin.org/articles/10.3389/fmicb. 2021.652863.
7. **Kapoor R, Salvadori M, Rafatullah M *et al.* (2021):** Exploration of microbial factories for the synthesis of nanoparticles – A sustainable approach for the bioremediation of environmental contaminants. Frontiers in Microbiology, 12:658294. https://doi.org/10.3389
8. **Abid J, Wark A, Brevet P *et al.* (2002):** Preparation of

silver nanoparticles in solution from a silver salt by laser irradiation. Chemical Communications, 7: 792-793.

9. **Jadoun S, Chauhan N, Zarrintaj P *et al*. (2022):** Synthesis of nanoparticles using microorganisms and their applications: A review. Environmental Chemistry Letters, 7 (3): 1-45.
10. **Medici S, Peana M, Coradduzza D *et al*. (2021):** Gold nanoparticles and cancer: Detection, diagnosis, and therapy. In Seminars in Cancer Biology, 76: 27-37.
11. **Thamer N, Adil B, Obaid A (2020):** Gold nanoparticles synthesis using environmentally friendly approach for inhibition human breast cancer. International Journal of Nanoscience, 19 (5):126-135.
12. **Mathews J, Forsythe A, Brady Z *et al*. (2013):** Cancer risk in 680 000 people exposed to computed tomography scans in childhood or adolescence: data linkage study of 11 million Australians. https://www.bmj.com/content/346/bmj.f2360.
13. **Rauf A, Imran M, Butt M *et al*. (2018):** Resveratrol as an anti-cancer agent: A review. Critical Reviews in Food Science and Nutrition, 58 (9): 428-447.
14. **Buzea C, Pacheco I, Robbie K (2007):** Nanomaterials and nanoparticles: sources and toxicity. Biointerphases, 2(4):17-71.
15. **Frebourg N, Nouet D, Lemée L *et al*. (1988):** Comparison of ATB staph, rapid ATB staph, Vitek, and E-test methods for detecting oxacillin heteroresistance in *Staphylococci* possessing *mecA*. Journal of Clinical Microbiology, 36 (1): 52-57.
16. **Sabir S, Zahoor M, Waseem M *et al*. (2020):** Biosynthesis of ZnO nanoparticles using *Bacillus subtilis*: characterization and nutritive significance for promoting plant growth in *Zea mays* L. https://journals.sagepub.com/doi/full/10.1177/ 1559325820958911
17. **Ali I, Jabir M, Al-Shmgani H *et al*. (2018):** Pathological and immunological study on infection with *Escherichia coli* in ale Balb/c mice. Journal of Physics: Conference Series, 1003 (1): 215-226.
18. **Khashan K, Badr B, Sulaiman G *et al*. (2021):** Antibacterial activity of Zinc Oxide nanostructured materials synthesis by laser ablation method. Journal of Physics: Conference Series, 1795 (1): 131-139.
19. **Al Salman H, Ali E, Jabir M *et al*. (2020):** *2-Benzhydrylsulfinyl-N-hydroxyacetamide-Na* extracted from fig as a novel cytotoxic and apoptosis inducer in SKOV-3 and AMJ-13 cell lines via P53 and caspase-8 pathway. European Food Research and Technology, 246 (8): 1591-1608.
20. **Jabir M, Sahib U, Taqi Z *et al*. (2020):** Linalool-loaded glutathione-modified gold nanoparticles conjugated with CALNN peptide as apoptosis inducer and NF-κB translocation inhibitor in SKOV-3 cell line. International Journal of Nanomedicine, 15: 9025-9047.
21. **Younus A, Al-Ahmer S, Jabir M (2019):** Evaluation of some immunological markers in children with bacterial meningitis caused by *Streptococcus pneumonia*. Research Journal of Biotechnology, 14: 131-133.
22. **Ismail E, Saqer A, Assirey E *et al*. (2018):** Successful green synthesis of gold nanoparticles using a *Corchorus olitorius* extract and their antiproliferative effect in cancer cells. International Journal of Molecular Sciences, 19 (9): 2612-2621.
23. **Langford J, Wilson A (1978):** Scherrer after sixty years: a survey and new results in determining crystallite size. Journal of Applied Crystallography, 11 (2): 102-113.
24. **Hong Bin W, Da L, Xue Y *et al*. (2018):** Pterostilbene (3',5'-dimethoxy-resveratrol) exerts potent antitumor effects in HeLa human cervical cancer cells via disruption of mitochondrial membrane potential, apoptosis induction and targeting m-TOR/PI3K/Akt signalling pathway. Journal of the Balkan Union of Oncology, 23 (5): 1384–1389.
25. **Al-Kalifawi E, Al-Azzawi Y (2017):** Silver nanoparticles synthesized by leaf extract of Khubaz (*Malva sylvestris*) and its antibacterial activity. Pro. of the 2nd Int. Sci. Conf. (1-2) Sothern Technical University, 20 (3): 1213-1233
26. **Al-Kalifawi E, Al-Azzawi Y, Hassan F (2018):** Biosynthesis of silver nanoparticles using Al-Ankabut's home extract and its antimicrobial activity. Academia Journal of Agricultural Research, 6 (5): 33-46.
27. **Sadalage P, Patil R, Havaldar D *et al*. (2021):** Optimally biosynthesized, PEGylated gold nanoparticles functionalized with quercetin and camptothecin enhance potential anti-inflammatory, anti-cancer and anti-angiogenic activitie. Journal of Nanobiotechnology, 19 (1): 84-91.
28. **Eustis S, Hsu H, El-Sayed M (2005):** Gold nanoparticle formation from a photochemical reduction of Au3+ by continuous excitation in colloidal solutions. A proposed molecular mechanism. The Journal of Physical Chemistry B, 109 (11): 4811-4815.
29. **Zare I, Yaraki M, Speranza G *et al*. (2022):** Gold nanostructures: synthesis, properties, and neurological applications. Chemical Society Reviews, 51: 2601-2680.
30. **Zhang X, Qu Y, Shen W *et al*. (2016):** Biogenic synthesis of gold nanoparticles by yeast *Magnusiomyces ingens* LH-F1 for catalytic reduction of nitrophenols. Colloids and Surfaces A: Physicochemical and Engineering Aspects, 497: 280–285.
31. **Sharma N, Pinnaka A, Raje M *et al*. (2012):** Exploitation of marine bacteria for production of gold nanoparticles. Microbial Cell Factories, 11 (1): 1-6.
32. **Lee Y, Ahn E, Park Y (2019):** Shape-dependent cytotoxicity and cellular uptake of gold nanoparticles synthesized using green tea extract. Nanoscale Research Letters, 14 (1): 129-137.
33. **Abdullah A, Mohammed A (2020):** Green synthesis of AuNPs from the leaf extract of Prosopis farcta for antibacterial and anti-cancer applications. Digest Journal of Nanomaterials and Biostructures, 15 (3): 943-951.
34. **McDougall R, Cahill H, Power M *et al*. (2022):** Multiparametric cytotoxicity assessment: the effect of gold nanoparticle ligand functionalization on SKOV3 ovarian carcinoma cell death. Nanotoxicology, 16 (3): 355-374.